CLAS12 Run-group H Experiments with a Transversely Polarized Target

Abstract

This document provides an update on the physics case and preparatory work for the C1 conditionally approved CLAS12 deep-inelastic scattering (DIS) experiments with a transversely polarized target, identified as run-group H.

Contents

1 Introduction

The CLAS12 run-group H (RGH) comprises 3 experiments approved with rating A by PAC39 to run for a total of 110 days with a 11 GeV beam scattering off a transversely polarized target.

- **C12-11-111** *Transverse spin effects in SIDIS at 11 GeV with a transversely polarized target using CLAS12*: a multi-dimensional analysis of the semi-inclusive (SIDIS) reactions to access transversity and tensor charge, and the Sivers and Collins functions connected with the spin-orbit phenomena of the strong-force dynamics [1];
- **C12-12-009** *Measurement of transversity with dihadron production in SIDIS with transversely polarized target*: a multi-dimensional analysis of the SIDIS reactions exploiting the dynamics of the di-hadron final state to access transversity in the banchmark collinear limit and investigate novel parton correlations inaccessible on the single hadron case [2];
- **C12-12-010** *Deeply Virtual Compton Scattering at 11 GeV with transversely polarized target using the CLAS12 Detector*: a multi-dimensional analysis of the DVCS reaction to access the most elusive Generalized Parton Distribution entering the orbital momentum sum rule (Ji sum rule) [3].

The experiments where approved with the C1 condition to address the technical issues related to the target performance with the laboratory management before scheduling [4].

All the three experiments were selected among the high-impact JLab measurements by PAC42 [5].

RGH experiments are precursor of EIC in one of the pillars of its physics program [6, 7]. Distinctive features in common of all the three experiments are the precise measurement of novel parton distributions and phenomena in an unexplored valence region where their magnitude could be maximal, a luminosity at least on order of magnitude higher than the precursor experiments, a large acceptance detector for the disentanglement of the various correlations and kinematic regimes, an excellent particle identification capability to access flavor sensitivity.

2 Physics Highlights

In the recent years, new parton distributions (PDFs) and fragmentation functions (FFs) have been introduced to describe the rich complexity of the hadron structure, focusing on the parton transverse degrees of freedom at the scale of confinement and moving toward the achievement of a 3D description of the parton dynamics. Relevant examples are transverse momentum dependent (TMD) and generalized (GPD) parton distributions, relating the longitudinal momentum fraction (referred to the direction of the hard probe) with the intrinsic partonic transverse momentum or position, respectively. Their detailed investigation requires a novel level of sophistication in the deep-inelastic scattering (DIS) experiments that should conjugate precision, in discriminating semi-inclusive and exclusive reaction details, and power, in collecting large amount of data to allow multi-dimensional analyses.

The CLAS12 run-group H program collects several fundamental measurements that provide access to elusive quantities and are only possible with the use of a transversely polarized target in conjunction with a large acceptance high-precision spectrometer.

The **Transversity** PDF describes the parton transverse polarization inside a transversely polarized nucleon, reflects the relativistic nature of the parton confinement and exhibits peculiar evolution properties. It is the less known leading PDF that does not vanish when integrated in the transverse momentum $k_\perp$, and can thus be studied in the collinear limit. Although essential for the nucleon description, due to its chirally-odd nature transversity has only recently been accessed in a limited kinematic range and with a large uncertainty that still prevents a reliable flavor decomposition [8]. Its first moment in Bjorken x, the tensor charge, is a fundamental quantity in quantum chromodynamics (QCD) connected to searches of beyond Standard Model phenomena such as the Electric Dipole Moment (EDM) of particles [9] and the tensor interaction [10]. CLAS12 data will cover an unexplored Bjorken-x interval in the valence region, providing unprecedented constraints to the tensor charge and allowing precise comparison with lattice QCD, which has made remarkable progresses in the past decades [11].

The **Sivers** PDF is a genuine TMD function which vanishes with $k_\perp$ integration. Among the most intriguing parton distributions, it requires a non-zero parton orbital angular momentum and a correlation with the nucleon spin. As a consequence of its non-trivial gauge-invariant definition, the Sivers function probes QCD at the amplitude level: it is naively T-odd (do not violate T-invariance due to the interaction phase) and exhibits a peculiar process dependence. A sign change is expected when moving from SIDIS to Drell-Yan processes, whose verification is one of the most urgent goals of the present experimental activity [8]. It is among the few TMDs that, while describing the non-perturbative nature when $k_\perp \ll Q^2$, should in principle match the perturbative regime with increasing transverse momentum, providing a formal bridge between the two QCD descriptions [12]. CLAS12 data will allow an extended coverage in the valence region and a disentaglement of the Sivers kinematic dependences, a crucial information for the study of these phenomena and the connections among different QCD regimes.

The **Collins** and **Di-hadron** FFs originate from spin-orbit effects connecting the spin of a fragmenting quark with the final observed hadron or di-hadron transverse momentum, respectively. Convincing evidences have been found for the existence of these mechanisms [8]. These peculiar FFs act as a polarimeter and allow to access the elusive chirally-odd distribution functions in SIDIS reactions. In particular the Di-hdaron FF, sensitive to the hadron pair *relative* transverse momentum, can be studied in the collinear limit providing a complementary access to transversity that does not depend on the TMD formalism, and can be reliably extended to the hadron-hadron scattering case [13]. High precision data from CLAS12 can complement present and future information gathered at the much higher center-of-mass energy of experiments at the e^+e^- colliders, like BELLE-II [14], and at hadron-hadron colliders, like PHENIX and STAR [15].

The **GPD E** describes asymmetries in the parton spatial distribution that imprint the underlying confinement dynamics. It it the least know GPD that enters the Ji sum rule quantifying the parton orbital momentum [16]. Its measurement in the golden deeply-virtual Compton scattering (DVCS) channel requires the usage of a transversely polarized target in case of protons, or the measurement of a beam spin asymmetry off an unpolarized target in case of neutrons [17]. As the latter is among the goals of RGB experiments that already took data, both measurements can be accomplished at CLAS12 providing an unprecedented level of information.

Since the last jeopardy review in 2020, few new results became available on the electro-production of mesons off a transversely polarized target. COMPASS published the study on di-hadron transverse-spin-dependent asymmetry on proton and deuterium targets [18], and the preliminary results on the deuteron data from 2022 run [19]. HERMES completed a multi-dimensional fit [20] and COMPASS a P_T-weighted analysis [21] of already published data. All these results are limited to Bjorken x below 0.3. COMPASS published Drell-Yan data consistent with the fundamental QCD prediction of a sign change of naive time-reversal-odd TMD PDFs (i.e. Sivers) when comparing the Drell-Yan process with SIDIS [22]. The interest in data on transversely polarized targets is manifest from the continue flow of phenomenological analyses of the sparse SIDIS data collected in the past couple of decades, in conjunction with proton-proton, e^+e^- and Drell-Yan data [23, 24]. No new DVCS results on transversely polarized targets became available after HERMES and this experiments provides the first chance to overcome the lack of information. New channels of investigation are being explored [25, 26] and phenomenological study is awaiting new inputs [27]. Lattice calculations are making steadly progresses [28, 29] and can offer benchmark quantities or complementary constraints to the phenomenological models.

3 The Transverse Target

The original target proposed for the Run Group H experiments was HDice, a frozen spin target of polarized solid hydrogen deuteride. However, it has been determined that this target system is not suitable for use in electron experiments, and so we will instead utilize a technology that has been successfully implemented in numerous experiments at Jefferson Lab, Dynamic Nuclear Polarization (DNP). This technique provides a number of advantages over the initial choice, including significantly higher polarization and much greater resistance to the depolarizing effects of the electron beam. Its drawbacks are target molecules with a greater fraction of unpolarized nucleons and a reliance on higher field, higher-uniformity magnets. Our decision is motivated below.

3.1 HDice in electron beams

As in all frozen spin targets, the nuclear spins in HDice are polarized in a high magnetic field and then placed in a lower field for data taking. During the experiment the polarization decays in an exponential manner towards a small, thermal equilibrium polarization governed by the sample temperature T and holding field B. The rate of this decay is characterized by the spin-lattice relaxation time T_1, which is also a strong function of both temperature and field. The relaxation time is also strongly affected by the presence of paramagnetic impurities within the sample. In fact, paramagnetic impurities are the dominant source of nuclear spin relaxation in most dielectric solids, and it is these impurities that eliminate HDice as a viable target for Run Group H.

Although the HDice concept dates to 1967 [30], its use in particle experiments has not been widespread and limited to two low-luminosity experiments with beams of real photons [31, 32]. Tests performed with charged particles have been discouraging, as HD samples with initially long relaxation times rapidly lost their polarization due to the radiolytic production of paramagnetic species in the material (predominately atomic H and D), combined with beam heating.

In 1975 Mano and Honig irradiated polarized solid HD at the Cornell Synchrotron with a pulsed beam (10 nA CW equivalent) of 10 GeV electrons [33]. The sample's relaxation time T_1 dropped from 8 hours to 15 minutes after 22 minutes of exposure. The authors found that melting and refreezing the HD sample restored its previous long value of T_1 and concluded that paramagnetic impurities such as atomic H and D were responsible for the depolarization.

In 2012 at Jefferson Lab, tests were performed in Hall B with a 6 GeV electron beam [34]. In the most prolonged exposure, an HD sample with $T_1 > 700$ hours lost 98% of its polarization after 14 hours at 1 nA. This corresponds to an average T_1 of about 3 hours. The polarization was completely destroyed by zeroing the magnetic holding field for one hour. When the field was reestablished, the polarization grew back to its previous value with the same 3 hour time constant, indicating permanent radiation damage from the beam.

Within the RGH development program, a series of detailed measurements were again performed at JLab using 8 MeV electrons from the Upgraded Injector Test Facility (UITF) [35]. A number of modifications were made to realize better performance: the magnetic holding field was increased from 0.3 T to 1.0 T, the sample was redesigned for improved heat removal, the beam current was reduced to 0.1–0.5 nA to maintain a lower sample temperature, and the beam raster frequency was increased from 1 Hz to 1000 Hz to minimize localized heating. Despite these efforts, the polarized sample was reduced to 37% ($1/e$) of its initial polarization after an accumulated charge of 15 μC. This corresponds to about 4 hour at 1 nA. It was also observed that the rate of polarization

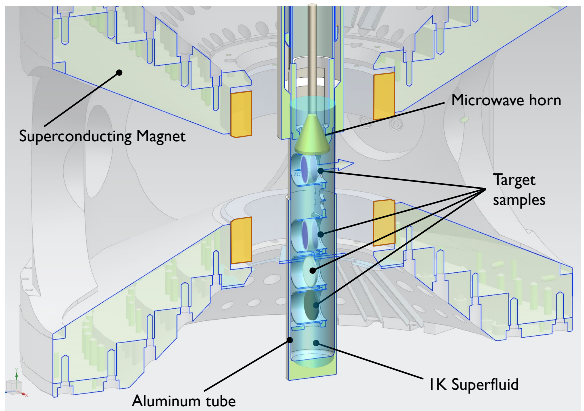

Fig. 1: Standard configuration of a target ladder for a DNP target system. Multiple samples (ammonia, carbon, polyethylene, empty, etc) are suspended in a bath of 1 K superfluid at the center of the polarizing magnet.

loss increased with accumulated dose and decreased when the heat from the beam was removed. Both are hallmarks of spin relaxation due to beam-induced paramagnetic impurities.

3.2 Dynamically polarized target

A more common and powerful alternative to HDice is dynamically polarized solid ammonia, NH_3 and ND_3. These polarized materials have been successfully utilized on multiple occasions at Jefferson Lab, with beam currents up to 140 nA [36], and with in-beam proton and deuteron polarizations exceeding 90% and 50%, respectively. One key to this material's success at Jefferson Lab is the fact that the paramagnetic impurities responsible for depolarizing frozen spin targets are actually used to dynamically *polarize* ammonia's nuclear spins.

In the case of ammonia, the amino radicals $\dot{N}H_2$ and $\dot{N}D_2$ are produced at concentrations of about 10^{-4} in the solid lattice by irradiation with an electron beam prior to the scattering experiment. These radicals are stable at temperatures below about 100 K, and so the samples can be indefinitely stored under liquid nitrogen until needed. Each radical has a single, unpaired electron whose spin can be highly polarized in more modest field and temperature conditions than those required for nuclear polarization. For example, at the 5 T, 1 K conditions of most JLab targets, the electron polarization exceeds 99% while the proton polarization is only 0.5%. This high electron polarization is then transferred to the nuclear spins using microwave-induced transitions in which both the electron and nuclear spins flip simultaneously. The nuclear polarization typically reaches its maximum value in less than two hours and can be selected to be positive or negative by adjusting the microwave frequency slightly below or above the electron spin resonance frequency.

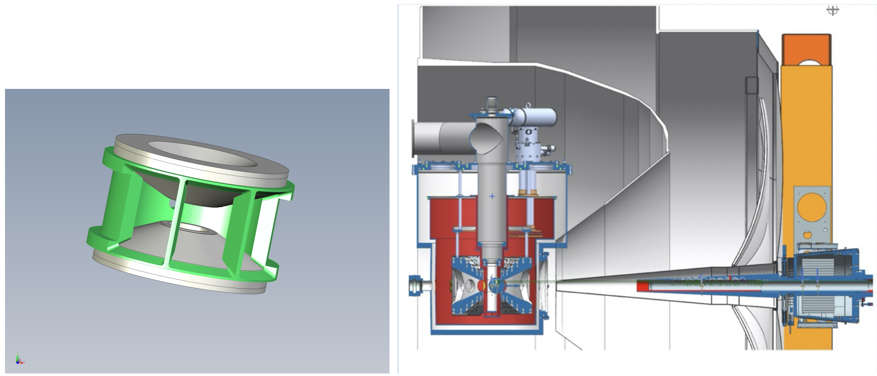

Fig. 2: Left: 3D model of the 5 T split-coil magnet for Run Group H. The opening in the forward directions for scattered particles spans $\pm 60°$ in the horizontal plane and $\pm 25°$ in the vertical. Right: Conceptual design showing the dynamically polarized target at the center of the CLAS12 HTCC.

During the scattering experiment, additional radical species such as atomic hydrogen are produced that are stable at the target's operating temperature of 1 K. These do not contribute to the dynamic polarization process, but do cause spin relaxation at an ever-increasing rate. As a result, the polarization decays in beam. However, this "radiation damage" can be largely repaired by annealing the sample at 90 K for several minutes. This is typically performed after a fluence (or dose) of about 5×10^{15} $e^{-}cm^{-2}$. Assuming a 2 nA beam current and 1.5 cm target diameter, this dose will be accumulated after approximately one week of beam time. More than one ammonia sample can be included on the target ladder, further increasing the time between anneals. With two ammonia samples, the overhead needed for the annealing process will be about 2–3%. Carbon and polyethylene samples can also be included on the ladder for dilution studies (Fig. 1).

3.3 Polarizing magnet

An obvious challenge to the operation of any transversely polarized target in Hall B is the *longitudinal* field produced by the CLAS12 solenoid. The original Run Group H proposals describe a solution using three sets of coils around the HDice target: a combination of solenoid and Helmholtz coils to negate the field of the CLAS12 solenoid, and saddle coils to generate a 0.5–1 T field in the vertical direction.

More recently, the use of the bulk superconductor magnesium diboride (MgB_2) has been explored. In this scenario, a hollow tube of MgB_2, surrounding the target sample, is cooled below its critical temperature while exposed to an external magnetic field transverse to the tube's axis. Upon removal from the external field, electrical currents are naturally generated within the superconducting walls to maintain the original transverse field in the tube's interior. As the target cryostat is moved into CLAS12 and the solenoid activated, the internal currents again adjust to exclude the longitudinal field and maintain the transverse. A test program at INFN Ferrara has shown promising results [37, 38], but the technology is not yet at the level of maturity needed for Run Group H. For example, it is not known if the technique can maintain the uniform, constant field needed for dynamic polarization.

In this document, we instead take a more simple and direct approach to the problem. The CLAS12 solenoid will be replaced by a superconducting, split-coil magnet similar to those previously used to polarize targets at JLab. The new coil will produce a 5 T field in the vertical direction and feature an opening that spans $\pm 60°$ in the horizontal plane and $\pm 25°$ in the vertical. A preliminary model of the magnet, as well as a conceptual design of the target cryostat inside the CLAS12 HTCC are shown in Fig. 2.

In order to compensate the bending of such a target holding magnet on the beam particles, a magnet chicane has been designed that can been realised with commercially available split-pair magnets, see Fig. 3.

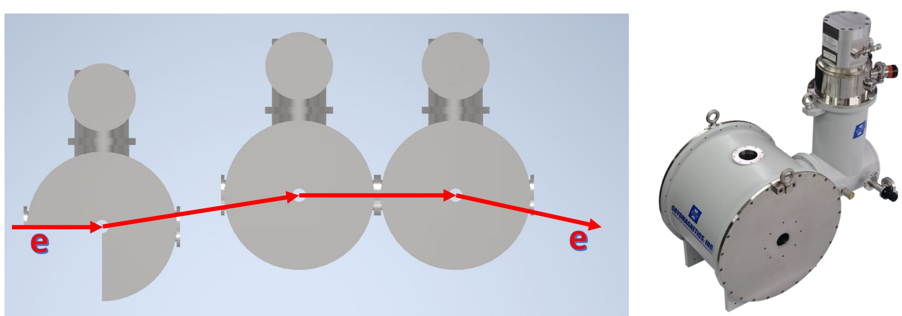

Fig. 3: (Left) The magnet chicane to compensate the beam bending of the target holding magnet (left). The 7.5T split-pair magnet from CryoMagnets inc. (right).

3.4 Target Figure-of-Merit

We can compare the new target design with the original HDice option by defining a figure-of-merit that reflects the time required to achieve a certain statistical precision in the measured scattering asymmetries:

$$\mathrm{FoM} = \mathcal{L}(1-\tau) f^2 P^2 \tag{1}$$

Here τ is the overhead needed for routine target operations, f is the target dilution factor, and P is the average target polarization. The luminosity $\mathcal{L}$ is the product of the beam intensity I/e and target thickness in nuclei per square

Quantity	HD	NH_3
(1-τ)	0.96	0.97
f	1/3	3/17
P	0.41	0.85
I (nA)	1.0	2.0
ρ (g/cc)	0.10	0.87
x (cm)	5.0	1.0
$\mathcal{L} \times 10^{33}$	2.5	5.0
FoM$\times 10^{32}$	0.4	1.1

Tab. 1: Comparison of solid HD and NH_3 as polarized target materials. The density of the materials has not been corrected for the aluminum wires used to cool solid HD ($15-20\%$ by weight) or the superfluid helium that cools solid ammonia (10% by weight). Details in the text.

centimeter:

$$\mathcal{L} = \frac{I}{e} x \rho N_A \tag{2}$$

x is the target length, ρ its density, and N_A is Avogadro's number.

The original proposals describe a 5 cm long HD target with a proton polarization of 60%. Although the results of the Cornell and Hall B beam tests were known at the time, no estimate of the rate of target depolarization was provided. This was clearly a concern to PAC-39, who therefore granted *conditional* approval to the proposals and stipulated that a spin relaxation time of 50 days or longer with a beam of 1 nA must be demonstrated for full approval. Starting at 60%, the polarization at the end of the 50 day lifetime will be reduced to 22%, giving an average value of about 41%. The HD target cannot be repolarized on the Hall B beamline but must instead be replaced. This requires a minimum of two days, giving an overhead of 4%. The dilution factor of protons in HD is 1/3.

In dynamically polarized NH_3, the overhead is dominated by the annealing process (3%), the dilution factor for polarized protons is 3/17, and an average polarization of 0.85 is assumed. This polarization was demonstrated during a 6 GeV experiment in Hall A using a polarized target similar to the one described here and a 10 nA beam current [39]. The luminosity will not be limited by the target operation in this case, but instead by the background produced by Moeller scattering. In Sec. 4.3 we argue that a conservative value is 5×10^{33} cm^{-2}s^{-1}. This corresponds to about 2 nA impinging on a 1 cm long NH_3 target.

The results are compared in Table 1. We see that the figure-of-merit for dynamically polarized ammonia is approximately three times higher than the PAC requirements for solid HD.

4 The CLAS12 Spectrometer

The CLAS12 spectrometer has been designed to run at high luminosity, up to about 3 orders of magnitude larger than the precursor experiments like HERMES and COMPASS, and bring the 3D nucleon structure study into the precision phase. CLAS12 started the data-taking with unpolarized hydrogen targets in spring 2018 and has so far succesfully run with different targets and detector configurations. In particular, CLAS12 successfully ran with longitudinally polarized NH_3 and ND_3 targets. Detailed calibration procedures and event reconstruction algorithms have been developed to reach a performance close to, or in same case superior of, the design specifications.

4.1 Forward Detector

With respect the goals of run-group H, the spectrometer has specifically demonstrated to be able to achieve the following performance.

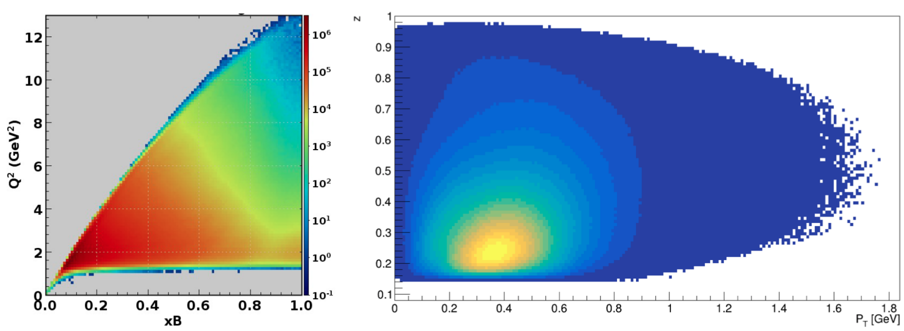

Fig. 4: (Left) The CLAS12 reach in the relevant kinematic variables at a beam energy of 10.6 GeV. (Left) Inclusive electron coverage in the hard scale Q^2 versus Bjorken x. (Right) Charged hadrons coverage in the transverse momentum P_T versus the fractional energy z.

Tracking The single track reconstruction efficiency has been improved with the implementation of ML algorithm to support effective denoising and track segment finding, to a level of better than 90% at the design luminsity of 1×10^{35} $\text{cm}^{-2}\text{s}^{-1}$, with a dependence of $98\% - 0.1 \times \text{I}$ in nA of beam current. The typical measured resolutions in the relevant kinematic quantities are $\Delta p/p = 0.67\%$, $\Delta\theta = 0.85$ mrad and $\Delta v_z = 4.6$ mm, in line with the design specifications of a resolution better than 1% in momentum and 1 mrad in polar angle [40].

Scattering Electron The efficiency of the CLAS12 trigger for DIS events, with the electron scattered inside the acceptance at an energy above 1.5 GeV, is greater than 99% [41]. Electrons are identified by a combination of signals in the Cherenkov counters and calorimeters. Thanks to the large acceptance of CLAS12, scattering electrons are detected in a wide kinematic range from elastic events to DIS with an extended reach at large values of Q^2, Bjorken x, and forward hadron kinematics, see Fig. 4.

Exclusive events A study is ongoing to exploit machine-learning techniques for the identification of exclusive DVCS events based on the electron and photon information provided by the CLAS12 Forward Detector but no (or partial) recoil information. Promising results have been obtained on RGA data, with physics observable comparable to the traditional analysis based on a complete recoil reconstruction.

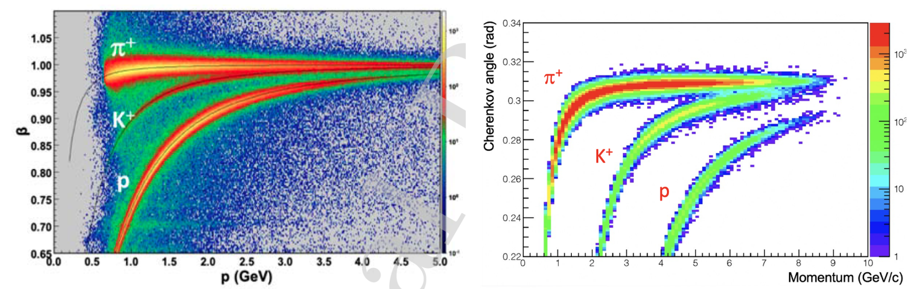

Fig. 5: (Left) The hadron separation provided by the Forward time-of-flight system. (Right) The hadron separation obtained by the RICH detector.

Hadron PID Identification of hadron particles is essential to gather flavor information in SIDIS observables. The CLAS12 forward time-of-flight system (FTOF) provides an excellent pion separation from kaons and protons at momenta up to about 3 GeV/c and 5 GeV/c [42], respectively, see left panel of Fig. 5. To complement such CLAS12 baseline configuration and provide hadron separation in the whole range of interest for SIDIS physics, up to momenta of 8 GeV/c, a ring-imaging Cherenkov detector (RICH) has been anticipated at the time of the proposal. The RICH has been designed as composed by two modules in a left-right symmetric configuration, to reduce the systematic effects in observables dependent on the target transverse polarization. The peculiar geometry of CLAS12 suggested an innovative hybrid-optics solution to limit the active area to about 1 m^2 per sector, with part of the light directly imaged and part of the light detected after reflection from mirrors. In order to limit the material inside the acceptance and realize a light but stiff structure, composite materials derived from aeronautic applications have been employed. Improvements have been pursued in all the components, achieving the world leading aerogel radiator clarity of 0.0050 $\mu m^4\, cm^{-1}$ at high refractive index (n=1.05), a 20% reduction of the aereal density of spherical mirrors in carbon fiber composite polymer with respect the LHCb realization, the first use of glass-skin planar mirrors in a nuclear physics experiment, the first use of the flat-panel multianode H12700 photomultiplier with a dynode structure dedicated to the single photon detection. The first module has been installed before the start of CLAS12 data taking and the RICH completed in 2022 before the start of the RGC polarized target run [43]. Ongoing data analysis shows that the CLAS12 RICH is able to match the required time and Cherenkov angle resolutions, and provide hadron separation in the wanted momentunm range, see right panel of Fig. 5.

4.2 Recoil Detection

The chosen magnet structure provides open acceptance in the angular region favored for recoil detection, up to 60 degrees (and beyond, thanks to the magnet bending). Protons below 30 degrees are anyway detected in the CLAS12 Forward Detector. In order to detect protons at larger angles, a dedicated recoil detector can be implemented. Such a detector does not pose a technological challenge and can be derived from already ongoing developments. Moreover the area to cover is limited, of the order of 30×60 cm^2.

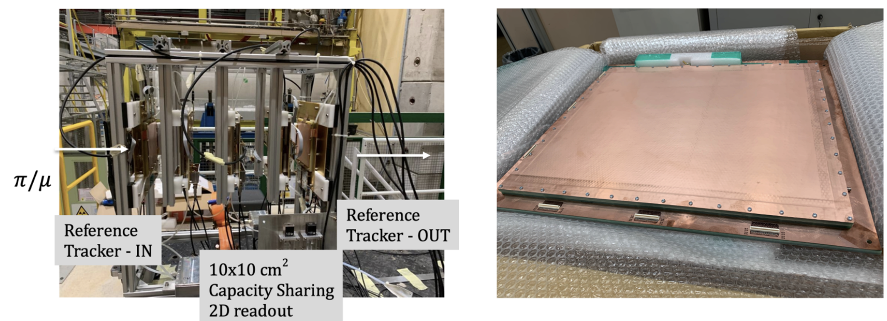

Fig. 6: Set-up used for testing the μ-Rwell performance during a test-beam at the SPS North Area H8C at CERN in June 2023 (left). Large area 40×46 cm^2 μ-Rwell prototype.

The tracking detector can be derived from the ongoing CLAS12 high-lumi project based on the μ-Rwell tracking technology. Several 10×10 cm^2 prototypes have been produced at INFN with 2D capacitive spreading readout achieving a spatial resolution of 100 μm and a time resolution of 20 ns. A large area 40×46 cm^2 prototype has also been realized and is now under test, see Fig. 6. The readout can be derived (and largely borrowed) from the readout of the GEM chambers produced at INFN for SBS in Hall-A, that are currently stored as spares but will become available after 2025. This readout is based on the chip APV25, the same chip in use for the μ-Rwell prototype tests. Alternatively, the same readout developed for the high-lumi project can be adopted.

To improve the time resolution to a sub-ns level, a scintillating fiber tracking layer readout by SiPM can be used. A prototype is being realized at INFN, see

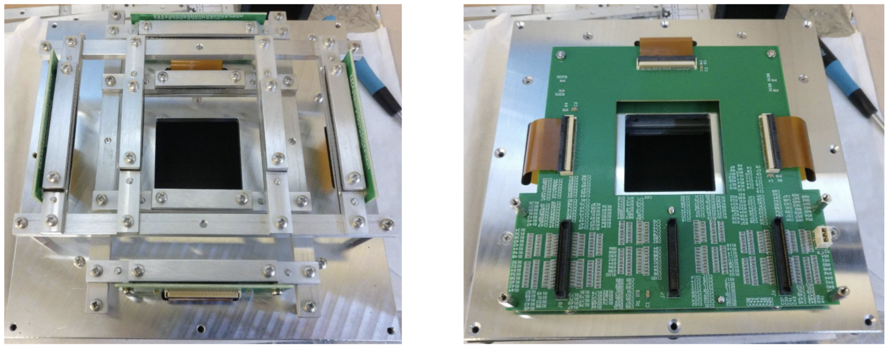

Fig. 7: The scintillating fiber tracking prototype under construction.

fig. 7. The readout can be derived (and largely borrowed) from the one of the CLAS12 RICH detector based on the MAROC3 chip. This readout has been already succesfully used with SiPM matrices for detecting signals down to few photon-electrons, achieving a single-photon time resolution of 0.5 ns largely driven by the FPGA settings. As alternative, the ALCOR readout being developed within the EIC dRICH R&D can easily reach the intrinsic resolution of the sensor, of the order of 100 ps.

4.3 Luminosity

The CLAS collaboration has completed experimental runs with both liquid hydrogen and deuterium targets, and has reached the design luminosity of $10^{35}\,\mathrm{cm}^{-2}\mathrm{s}^{-1}$ with a deuterium target and 45 nA electron beam current. This is much higher than the luminosity $\mathcal{L} = 5 \times 10^{33}\,\mathrm{cm}^{-2}\mathrm{s}^{-1}$ assumed for the RGH experiments. The ongoing high-lumi project aims to complement the CLAS12 tracking with a front layer of micro-Rwell detectors, able to improve the spatial resolution and rate capability of CLAS12 tracking in the most critical region close to the interaction point, and support a factor two increase in luminosity.

With a dynamically polarized ammonia target, the luminosity is no longer limited by the target polarization lifetime, but by the background induced on the open-acceptance spectrometer. CLAS12 has measured the hit occupancy levels in the Drift Chambers (DC), the most sensitive detectors, as a function of the beam intensity and solenoid current. The typical occupancy is driven by Moeller scatterings in the target and secondary interactions in the shielding around the downstream beam pipe, in the detector structure and in the air filling the Hall. CLAS12 simulations reproduce data within an acceptable 30% level.

For the RGH experiments, where the CLAS12 solenoid is replaced by the target 5T transverse polarizing field, the Moeller backgroud is no longer contained inside the beam pipe, but is mainly trapped inside the target region. The baseline of the RGH experiments is to run with no Forward Tagger (FT-OFF) and with additional shielding elements installed to minimize the secondary interactions.

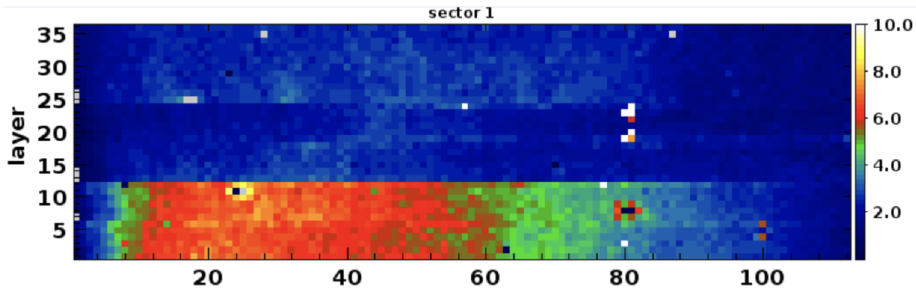

Fig. 8: Typical RGC occupancies as measured by CLAS12 the online monitor during the RGC run with a NH_3 target.

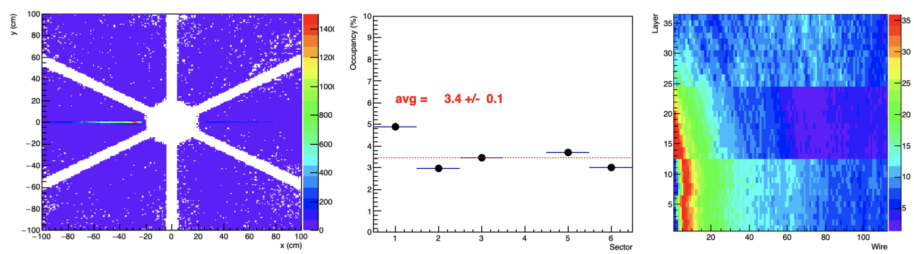

Fig. 9: Simulation results at the nominal RGH luminosity. Background hit distribution on the first DC tracking layer with visible the so-call sheet-of-flame in sector 4 (left). Mean hit occupancy for all DC layers but 4 (center). Hit occupancy per single layer and wire on sector 4 (right).

The RGH background has an additional peculiar component, due to the energy loss of the beam particles passing without interaction through the target. If the loss is big enough, the particle is bent outside the pipe and into the detector acceptance. Such a background is concentrated in the bending plane of the 5T target magnet, creating the so-called *sheet-of-flame*, see Fig. 9 (left). With a vertical magnetic field, the sheet-of-flame will illuminate sector 4 to a level that could be hardly sustainable with the present DC readout, able to record just a single hit in the extended readout gate (between 0.5 μs and 1.5 μs depending on the drift cell size). As a conservative approach, this work assumes to switch off sector 4, and operate with the other 5 sectors up to a maximum tolerable occupancy rate of 6-8% as already achieved (even with higher occupancy hot-spots) during the RGC data-taking on longitudinally polarized NH_3 and xND_3

targets , see Fig 8. This corresponds to the design RGH luminosity of 5×10^{33} $\mathrm{cm}^{-2}\mathrm{s}^{-1}$, once a conservative factor 2 is used to account for the different DC readout gates in simulations, see Fig. 9 (center), and real data.

There are concrete possibilities to exceed the conservative luminosity estimate above. RGH will benefit from the ongoing tracking improvements based on machine learning techniques [44, 45]. With the addition of the micro-Rwell tracking layer under development for the CLAS12 high-lumi project, a significant improvement in luminosity is expected (up to a factor two). Optimization studies are ongoing to adapt the CLAS12 background shielding to RGH. Possible mitigation measures can be introduced to partially operate sector 4. These includes switching off just the wires close to the beam where the background particles concentrate, see Fig. 9 (right), veto the events with multiple particles as resolved by the high-lumi tracking layer, upgrade the DC readout to process multiple hits in the readout gate. An interesting option is to rotate the target by 90 degrees in order to match the sheet-of-flame with the torus coil shadow. All these developments are being pursued to maximize the physics output of RGH experients, with the possibility to overcome what has been projected at the time of the proposal.

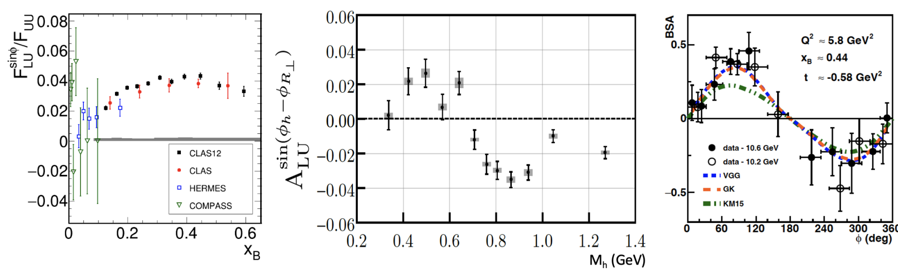

Fig. 10: CLAS12 published results on beam spin asymmetry observables based on just a fraction of the recorded statistics. SIDIS π^+ asymmetry as a function of Bjorken x compared to previous results [46] (left), SIDIS di-hadron asymmetry find not-zero for the first time [47] (center), DVCS asymmetry as a function of the azimuthal angle ϕ compared to phenomenological models [48] (right).

5 Physics Observables

Physics analyses are in progress based on the 10.6 GeV data. CLAS12 results for both the SIDIS and exclusive channels have been published by the Collaboration and presented at the conferences. As example, published beam spin asymmetry of SIDIS π^+, SIDIS di-hadron and DVCS events, based on a fraction of the recorder statistics, are shown in Fig. 10. Data confirm that CLAS12 allows a much extended reach inside the DIS regime (large Q^2) with respect CLAS and the valence region (large x) with respect previous experiments, with an unprecedented statistical precision. With the improved knowledge of the instrumental effects, and the refinement of the calibration procedures and reconstruction algorithms, further progresses are expected towards the best CLAS12 performance before the start of RGH experiments.

5.1 Semi-inclusive Physics

Due to the definition of an orthogonal direction, transverse single spin asymmetries are key for the access of transverse momentum dependent parton distribution functions (TMDs) [49]. The extraction of TMDs are a focus of the nuclear physics community to access the 3D momentum structure of the proton. Fig. 11 shows exemplary different global extractions of transversity. The precision of the extractions and their compatibility becomes worse in the valence quark region. This is due to the lack of data for $x >\approx 0.3$. Since the magnitude of transversity is peaking in the same region,this leads to significant uncertainties on the tensor charge, the integral over transversity. The tensor charge can be compared with lattice calculations and is also needed to calculate couplings in certain scenarios of new physics with tensor coupling. On the right panel in Fig. 11 world data for the longitudinal beam spin asymmetries (BSAs) compared with CLAS12 BSA extraction from RGA is shown. We expect as similar x coverage for RGH. It can be seen that CLAS12 covers up to $x \approx 0.6$. This would cover e.g. the whole peak structure in current transversity extractions. Other TMDs like Sivers are also dominated by the valence region, thus a similar argment for the importance of the CLAS12 TSSAs holds.

5.2 DVCS

Measuring DVCS on a transversely polarized proton target is crucial as the transverse-target spin asymmetry (TTSA) is the DVCS observable having the strongest sensitivity to the GPD E of the proton. Knowing E is paramount in order to extract the quarks' angular momentum contribution to the proton spin via the Ji sum rule.

Projections for the DVCS TTSA that will be obtained by RGH have been computed using a data-driven method to estimate the yields. Proton-DVCS yields (Y) were extracted using data from the RGA Fall 2018 period. Acceptances were computed for both the RGH and the RGA configurations. The RGA yields were multiplied, for each kinematic bin in $(Q^2, x_B, -t, \phi)$, by the ratio of the RGH and RGA acceptance for pDVCS, obtained from full gemc simulations. This product was then multiplied by the ratio of the integrated luminosities of RGH and RGA. This is summarized in Eq. 3.

$$Y_{RGH} = Y_{RGA} * \frac{Acc_{RGH} * L_{RGH}}{Acc_{RGA} * L_{RGA}} \cdot \frac{3}{17}, \tag{3}$$

where $L_{RGH} = 100$ days $\cdot 5 \cdot 10^{33}$ cm^{-1}s^{-1}, $L_{RGA} = 16$ days $\cdot 0.8 \cdot 10^{35}$ cm^{-1}s^{-1}, and the factor $3/17$ accounts for the fraction of protons from hydrogen in NH_3.

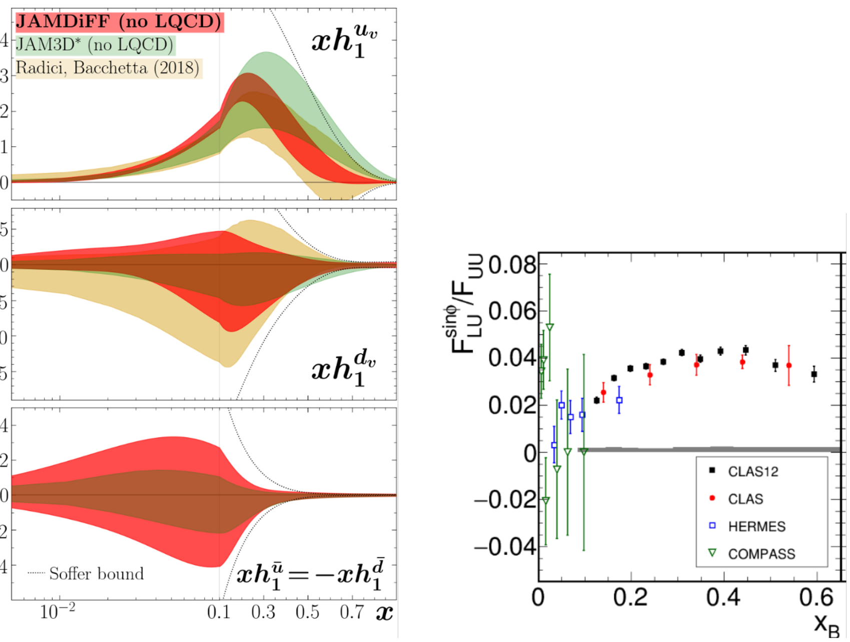

Fig. 11: Left: Current extractions of transversity from SIDIS, pp and e^+e^- data. Figure from [50]. Right: Beam spin asymmetries measured by CLAS12 compared with world data. Legacy data is limited to $x < 0.3$. This lack of data in the valence region explains the larger uncertainty and difference between the transversity extractions.

The grid of 4-dimensional bins was established according to the statistics obtained with Eq. 3. The TTSA was computed, as a function of ϕ, at the average kinematics of each $(Q^2, x_B, -t)$ using the VGG model. The obtained yields for RGH were used to deduce statistical error bars for the TTSA, according to the formula:

$$\sigma_A = \frac{1}{P} \cdot \sqrt{\frac{1 - (P \cdot A)^2}{Y_{RGH}}}, \tag{4}$$

where A is the value of the TTSA, and P is the target polarization, assumed to be 85%.

The projections for the TTSA are shown in Fig. 12.

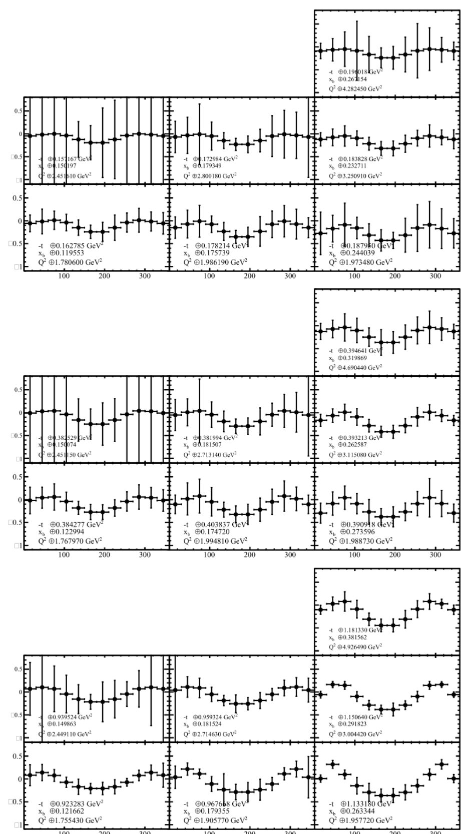

Fig. 12: Projections for the transverse target spin asymmetry versus ϕ which will be obtained by RGH for the proton-DVCS reaction, for three bins in $-t$ (each block of 7 plots, from top to bottom), for 3 bins in x_B (along the horizonthal axis), and 3 bins in Q^2 (along the vertical axis). The average kinematics is indicated on each plot.

6 Summary

The RGH experiments at CLAS12 offer a compelling physics program that have the potential to provide unprecedented information on the peculiar parton dynamics within the nucleon and during fragmentation. Since the approval in 2012, the interest in this field of research has worldwide grown and culminated with the start of the EIC Project, the theoretical understanding and lattice calculations have make important progresses and consolidate the interest in new experimental results. At the same time, a comprehensive program has been pursued at JLab to understand and overcome the technical challenges connected with running a transversely polarized target inside CLAS12 that is based on the concrete experience acquired so far running the experiment. We request the PAC to allow the conclusion of this effort and confirm the conditionally approved beam time (110 days).

References

[1] H. Avakain et al., *Transverse spin effects in SIDIS at 11 GeV with a transversely polarized target using the CLAS12 Detector.* https://www.jlab.org/exp_prog/proposals/12/C12-11-111.pdf.

[2] H. Avakain et al., *Measurement of transversity with dihadron production in SIDIS with transversely polarized target.* https://www.jlab.org/exp_prog/proposals/12/PR12-12-009.pdf.

[3] H. Avakian et al., *Deeply Virtual Compton Scattering at 11 GeV with transversely polarized target using the CLAS12 Detector.* https://www.jlab.org/exp_prog/proposals/12/PR12-12-010_rv.pdf.

[4] PAC39 Report, https://www.jlab.org/exp_prog/PACpage/PAC39/PAC39%20Final_Report.pdf.

[5] PAC42 High-Impact Selection, https://www.jlab.org/exp_prog/PACpage/High_Impact_Proposals.pdf.

[6] A. Accardi et al., *Electron Ion Collider: The Next QCD Frontier : Understanding the glue that binds us all*, Eur.Phys.J.A 52 (2016) 9, 268.

[7] R. Abdul Khalek et al., *Science Requirements and Detector Concepts for the Electron-Ion Collider: EIC Yellow Report*, Nucl. Phys. A, 1026 (2022) 122447.

[8] H. Avakian, A. Bressan and M. Contalbrigo, *Experimental results on TMDs*, Eur. Phys. J. A52 (2016) 6, 150.

[9] M. Pitschmann et al., *Nucleon tensor charges and electric dipole moments*, Phys. Rev. D91 (2015) 074004.

[10] A. Courtoy et al., *Beyond-Standard-Model Tensor Interaction and Hadron Phenomenology*, Phys. Rev. Lett. 115 (2015) 162001.

[11] C. Alexandrou, *Recent progress on the study of nucleon structure from lattice QCD and future perspectives*, SciPost Phys. Proc. 3 (2020) 015.

[12] A. Bacchetta et al., *Matches and mismatches in the descriptions of semi-inclusive processes at low and high transverse momentum*, JHEP 08 (2008) 023.

[13] M. Radici and A. Bacchetta, *First Extraction of Transversity from a Global Analysis of Electron-Proton and Proton-Proton Data*, Phys.Rev.Lett. 120 (2018) 19, 192001.

[14] I. Garzia and F. Giordano, *Transverse-momentum-dependent fragmentation functions in e^+e^- annihilation*, Eur. Phys. J. A52 (2016) 6, 152.

[15] M.J. Skoby, *High Precision Measurement of Transversity Using Di-hadron Correlations in $\vec{p}-p$ Collisions at $s_{NN} = 500$ GEV.*, Int. J. Mod. Phys. Conf. Ser. 40 (2016) 1660038.

[16] L. Adhikari and M. Burkardt, *Angular Momentum Distribution in the Transverse Plane*, Phys. Rev. D94 (2016) 11, 114021.

[17] N. d'Hose, S. Niccolai and A. Rostomyan, *Experimental overview of Deeply Virtual Compton Scattering*, Eur. Phys. J. A52 (2016) 6, 151.

[18] G.D. Alexeev et al. (COMPASS), *Transverse-spin-dependent azimuthal asymmetries of pion and kaon pairs produced in muon-proton and muon-deuteron semi-inclusive deep inelastic scattering*, Phys. Lett. B, 845 (2023) 138155.

[19] G.D. Alexeev et al. (COMPASS), *High-statistics measurement of Collins and Sivers asymmetries for transversely polarised deuterons*, e-print arXiv: 2401.00309.

[20] A. Airapetian et al. (HERMES), *Azimuthal single- and double-spin asymmetries in semi-inclusive deep-inelastic lepton scattering by transversely polarized protons*, JHEP 12 (2020) 010.

[21] G.D. Alexeev et al (COMPASS), *Measurement of P_T-weighted Sivers asymmetries in leptoproduction of hadrons*, Nucl. Phys. B 940 (2019) 34-53.

[22] G.D. Alexeev et al. (COMPASS), *Final COMPASS results on the transverse-spin-dependent azimuthal asymmetries in the pion-induced Drell-Yan process*, e-print arXiv: 2312.17379.

[23] C. Cucuzza et al., *Transversity Distributions and Tensor Charges of the Nucleon: Extraction from Dihadron Production and Their Universal Nature*, Phys. Rev. Lett. 132 (2024) 9, 091901.

[24] M. Boglione et al., *Simultaneous reweighting of Transverse Momentum Dependent distributions*, e-print arXiv: 2402.12322.

[25] B. Bessidskaia et al., *Recoil proton polarization: A new discriminative observable for deeply virtual Compton scattering*, Phys. Rev. D, 107 (2023) 1, 014020.

[26] M. Defurne et al. (Hall-C), *Recoil Nucleon Polarization in Deeply Virtual Compton Scattering and Neutral Pion Electroproduction in Hall C*, LOI12-23-014, https:www.jlab.orgexp_progproposals23LOI12-23-014.pdf.

[27] M. Čuić et al., *Separation of Quark Flavors Using Deeply Virtual Compton Scattering Data*, Phys. Rev. Lett. 125 (2020) 23, 232005.

[28] C. Alexandrou et al., *Moments of the nucleon transverse quark spin densities using lattice QCD*, Phys. Rev. D, 107 (2023) 5, 054504.

[29] A. Scapellato et al., *Proton generalized parton distributions from lattice QCD*, Rev. Mex. Fis. Suppl., 3 (2022), 3, 0308104.

[30] A. Honig, *Highly Spin-Polarized Proton Samples – Large, Accessible, and Simply Produced*, Phys. Rev. Lett. 19 (1967) 1009.

[31] S. Hoblit et al., *Measurements of* $\vec{\mathbf{H}}\vec{\mathbf{D}}$ $(\vec{\gamma},\pi)$ *and Implications for the Convergence of the Gerasimov-Drell-Hern Integral*, Phys. Rev. Lett. 102, 172002 (2009).

[32] D. Ho et al., *Beam-Target Helicity Asymmetry for* $\vec{\gamma}\vec{n} \rightarrow \pi^- p$ *in the* N^* *Resonance Region*, Phys. Rev. Lett. 118, 242002 (2017).

[33] H. Mano and A. Honig, *Resistance of Solid HD Polarized Proton Targets to Damage from High-Energy Proton and Electron Beams*, Nucl. Instrum. Methods Phys. Res. **124** (1975) 1.

[34] M.M. Lowry et al., *Electrons on the HDice Target: Results and Analysis of Test Runs at JLab in 2012*, Published in PoS(PSTP 2013)015.

[35] Kevin Wei, *The Response of Polarized Protons in Solid Hydrogen-Deuteride (HD) to Electron Beams*, Ph.D. Thesis, University of Connecticut (2021).

[36] C.D. Keith, *Polarized Solid Targets at Jefferson Lab*, Proceedings of PSTP2015, The XVI International Workshop in Polarized Sources, Targets, and Polarimetry, PoS(PSTP2015)013.

[37] M. Statera et al., *A bulk superconducting magnetic system for the CLAS12 target at Jefferson Lab*, IEEE Trans. Appl. Supercond. 115 (2015) art. n. 4501004.

[38] M. Statera et al, *Magnetic System for the CLAS12 Proposals*, IEEE Trans. Appl. Supercond. 23 (2013) art. n. 3800304.

[39] J. Pierce et al., *Dynamically polarized target for the and* g_2^p *and* G_E^p *experiments at Jefferson Lab*, Nucl. Instr. Meth. Phys. Res. A 738, 54 (2014).

[40] V.D. Burkert et al., *The CLAS12 Spectrometer at Jefferson Laboratory*, Nucl. Instrum. Meth. Phys. Res. A 959 (2020) 163419.

[41] B. Raydo et al., *The CLAS12 Trigger System*, Nucl. Instrum. Meth. Phys. Res. A 960 (2020) 163529.

[42] D. Carman et al., *The CLAS12 Forward Time-of-Flight system*, Nucl. Instrum. Meth. A, 960 (2020) 163629.

[43] M. Contalbrigo et al., *The CLAS12 Ring Imaging Cherenkov detector*, Nucl. Instrum. Meth. Phys. Res. A 964 (2020) 163791.

[44] P. Thomadakis et al., *Using machine learning for particle track identification in the CLAS12 detector*, Comput. Phys. Commun., 276 (2022) 108360.

[45] P. Thomadakis et al., *De-noising drift chambers in CLAS12 using convolutional auto encoders*, Comput. Phys. Commun., 271 (2022) 108201.

[46] S. Diehl et al. (CLAS12), *Multidimensional, High Precision Measurements of Beam Single Spin Asymmetries in Semi-inclusive* π^+ *Electroproduction off Protons in the Valence Region*, Phys. Rev. Lett. 128 (2022) 6, 062005.

[47] T.B. Hayward et al. (CLAS12), *Observation of Beam Spin Asymmetries in the Process* $ep \rightarrow e'\pi^+\pi^- X$ *with CLAS12*, Phys. Rev. Lett. 126 (2021) 152501.

[48] G. Christiaens et al. (CLAS12), *First CLAS12 Measurement of Deeply Virtual Compton Scattering Beam-Spin Asymmetries in the Extended Valence Region*, Phys. Rev. Lett. 130 (2023) 21, 211902.

[49] M. Anselmino, A. Mukherjee and A. Vossen, *Transverse spin effects in hard semi-inclusive collisions*, Prog. Part. Nucl. Phys. **114**, 103806 (2020).

[50] C. Cocuzza et al. [Jefferson Lab Angular Momentum (JAM)], *First simultaneous global QCD analysis of dihadron fragmentation functions and transversity parton distribution functions*, Phys. Rev. D **109**, no.3, 034024 (2024).